The effect of different surface treatment methods on the adhesion and corrosion resistance of metal protective coatings

Zora Goodwin[1]

[1]University of Alaska

***Corresponding Author:**
drzoragoodwinjr@gmail.com,
dgoodwin4@alaska.edu

Received: 18/01/2025
Revised: 11/3/2025
Accepted: 16/05/2025
Published: 30/06/2025

Abstract: This study systematically investigated the effects of three types of surface modification techniques—chemical treatment, thermal treatment, and electrochemical treatment—on the adhesion and corrosion resistance of SiO_2 protective coatings on TC4 titanium alloy substrates. Through multi-scale characterization, it was found that substrate roughness is positively correlated with coating adhesion. C_8HO_3Si chemical treatment (roughness 63 μm) and MAO treatment (62 μm) achieved the highest adhesion strengths of 8.01 MPa and 7.91 MPa, respectively, with both exhibiting 100% Type B interface failure (cohesive failure within the coating), indicating that the interface bonding strength exceeds the coating's inherent strength. In contrast, H_2O_2 treatment (roughness 16 μm) exhibited the lowest adhesion (2.57 MPa). Electrochemical testing revealed that C_8HO_3Si-treated samples had the most positive corrosion potential (-0.087 V), lowest corrosion current (4.3 nA/cm^2), and widest passivation range (0.131 V), demonstrating the best corrosion resistance. MAO treatment increased surface hardness to 417 HV (uncoated substrate: 204 HV), improving corrosion resistance by 51.08%. After 10 days of salt spray testing, the impedance of the C_8HO_3Si and MAO coating systems remained above $1.0 \times 10^9\ \Omega \cdot cm^2$, significantly outperforming FCS treatment (corrosion current: 30.7 nA/cm^2). XRD confirmed that MAO forms highly crystalline rutile-type TiO_2 (characteristic peaks at 27.5° and 36.1°), while FCS generates a $CaTiO_3$/hydroxyapatite composite layer (peaks at 33.2° and 25.9°). The dense phase structure is key to enhancing protective performance. The synergistic optimization of substrate roughness, interfacial bonding, and passivation capability achieved by combining C_8HO_3Si chemical treatment with MAO electrochemical treatment provides an effective solution for the application of titanium alloy protective coatings in harsh environments.

Keywords: metal protective coatings, titanium alloy surface treatment, C_8HO_3Si, corrosion resistance, micro-arc oxidation, electrochemical impedance

1 | Introduction

Metal corrosion issues are prevalent across many sectors of the national economy, such as oil and gas, petrochemicals, transportation, and machinery manufacturing. In fact, corrosion problems exist wherever metal

materials are used [1, 2]. Corrosion causes significant losses and harm to social production. According to rough estimates, the global economic losses caused by metal corrosion have reached 2.5 trillion US dollars. In the past, looking at the global oil and gas production industry, according to estimates by the American Society for Testing and Materials, the annual total corrosion cost worldwide was 1.3 billion dollars [3]. The annual losses from metal corrosion far exceed the combined losses from floods, fires, windstorms, and earthquakes (average values), and this does not include indirect losses caused by corrosion-related shutdowns, reduced production, and explosions [4, 5, 6]. Moreover, corrosion-related safety incidents cannot be ignored. For example, a hydrogen sulfide stress corrosion-induced rupture of a reflux tank at a petrochemical plant led to an explosion, resulting in direct economic losses of nearly 9 million yuan and causing casualties [7, 8]. Additionally, corrosion leads to extensive rusting, causing premature failure of metal materials and resulting in significant waste of resources and energy [9]. Corrosion products and deposits reduce the heat transfer efficiency of equipment such as boilers and heat exchangers, wasting large amounts of standard coal. The harmful gases such as SO_2 produced by burning this coal further exacerbate environmental pollution [10, 11, 12]. Therefore, to protect metals from corrosion, applying a coating to the metal surface is one of the commonly used methods.

Metal coatings are an economical and effective material for protecting metals. Under the coating, the likelihood of electrochemical corrosion of the metal decreases, as the coating blocks the source of corrosion between the metal and atmospheric corrosive substances, allowing the metal to retain its original properties [13, 14, 15]. However, the protective effect of metal coatings is not foolproof; coated metals may still be subject to corrosion, aging, and inadequate adhesion, leading to failure. Coating failure is often caused by cathodic reactions or reactants affecting the coating on the metal surface. These reactions directly lead to the separation of the coating from the metal, a phenomenon known as cathodic delamination [16, 17]. Cathodic reactions can occur under natural corrosion conditions or under protective conditions. However, regardless of the condition, when the pH value in the cathodic zone reaches 13–14, it indicates that the external environment has become strongly alkaline, which is a highly aggressive metal oxide that easily attacks the coating on the metal surface [18, 19]. When atmospheric conditions change and coating-metal separation occurs, the metal exhibits rust-like colors, indicating that the coating oxides have been damaged by strong alkaline substances, thereby losing their protective efficacy [20, 21]. This has also been confirmed in some coating scratch tests, where strong alkaline substances can erode the polymer molecules in the coating, causing it to become brittle, crack, and fail [22]. Additionally, during corrosion, hydroxide ions are generated at the cathode, which can hydrolyze certain water-soluble groups in the paint film, disrupting the wet adhesion between the coating and the metal. This causes the paint film to lose its original mechanical and physical properties, thereby losing its protective function for steel [23, 24, 25]. In this context, researchers have focused on improving the adhesion and corrosion resistance of metal protective coatings through various surface treatment methods.

To improve adhesion between metal and coating, Baek et al. [26] used 3D printing technology to modify the surface of polyetheretherketone (PEEK) materials, resulting in reduced peel strength of the metal coating, indicating that this method enhances adhesion. Caraguay et al. [27] described using laser surface texturing before organic coating deposition to improve adhesion between organic coatings and steel. Similarly, Fan et al. [28] used a laser surface texturing process with a 500-volt voltage to treat aluminum alloy ceramic coatings, achieving the strongest adhesion after 30 minutes of treatment. Abdelaal et al. [29] employed air plasma treatment during the deposition of polymer coatings on metal substrates, achieving higher adhesion and friction performance.

To enhance the corrosion resistance of metal coatings, Dong et al. [30] subjected high-speed laser-clad nickel/316L alloy coatings to heat treatment, improving corrosion resistance. However, corrosion resistance first

increased and then decreased with rising treatment temperatures. Gao et al. [31] proposed a surface treatment technique—ultrasonic impact treatment—to enhance the performance of high-entropy alloy coatings, improving corrosion resistance by 23% while also enhancing wear resistance and tensile strength. Wang et al. [32] applied magnetron sputtering and remote induction-coupled oxygen plasma treatment to multi-layer chromium coatings, resulting in a decrease in the corrosion rate of stainless steel coated with chromium oxide layers and an improvement in the corrosion resistance of the coatings. Izadi et al. [33] demonstrated that the corrosion resistance of low-carbon steel surfaces coated with epoxy coatings after treatment with environmentally friendly sol-gel films was improved.

To enhance adhesion and corrosion resistance, Parhizkar et al. [34] used graphene oxide nanosheets and 3-aminopropyl triethoxysilane to covalently modify the steel surface, significantly improving the adhesion and corrosion resistance of the epoxy coating and reducing cathodic delamination. Ramezanzadeh et al. [35] treated steel surfaces with epoxy coatings using environmentally friendly praseodymium oxide nanomembranes, significantly improving corrosion resistance and bond strength while reducing cathodic delamination. Mahidashti et al. [36] improved the corrosion resistance and adhesion properties of epoxy coatings on steel surfaces treated with cerium conversion coatings and nettle inhibitors. Iqbal et al. [37] subjected AA2024-T3/organic coatings to continuous polyetheroxane and citric acid dehydrogenase surface treatment, achieving better wet adhesion and corrosion resistance. Bahlakeh et al. [38] treated low-carbon steel polyester/melamine coatings with neodymium oxide nanomembranes, significantly reducing the peeling rate and improving corrosion resistance. The adhesion strength of coatings treated with neodymium oxide/hydroxide compounds also increased. Jothi et al. [39] reported that the adhesion and corrosion resistance of AZ31 magnesium-based polyurethane coatings were improved after anodic oxidation treatment. Wang et al. [40] modified the silane coupling agent-treated micro-arc oxidation layer on water-based polyurethane coatings on aluminum alloys, resulting in significantly improved adhesion and corrosion resistance. Trentin et al. [41] noted that mechanical polishing, etching, sol-gel primer, and anodic oxidation treatment can all enhance the adhesion and corrosion resistance of epoxy coatings on low-carbon steel and aluminum, with aluminum showing the best results after anodic oxidation treatment.

The article provides a detailed exposition of various surface treatment technologies for titanium alloys, microstructural interface characterization methods, and testing methods for key coating properties. Specifically, in terms of surface treatment technologies, the research focuses on three core methods: chemical treatment, thermal treatment, and electrochemical treatment. The systematic application of these methods aims to provide diverse substrate surface states with distinct characteristics for subsequent coating applications. After determining the processing methods, phase composition, microstructure, and elemental distribution at the interface between the coating and substrate before and after processing were comprehensively analyzed using techniques such as XRD, optical microscopy, scanning electron microscopy (SEM), and electron probe microanalysis (EPMA). Additionally, substrate property tests quantified the fundamental parameters influencing coating adhesion, including surface roughness and Vickers hardness. Finally, the interface bonding performance was assessed through multi-scale mechanical testing methods such as scratch tests, indentation tests, and tensile tests to thoroughly investigate the bonding quality between the coating and substrate. The final performance tests directly targeted the core functional properties of the coating. Adhesion tests quantitatively measured the coating's resistance to vertical peeling. Toughness tests evaluated the coating's resistance to bending deformation to determine the optimal toughness corresponding to the pivot size. To evaluate corrosion resistance, accelerated tests simulating a corrosive environment were designed. Chloride salt immersion tests were conducted in a 3.0% NaCl solution to observe the corrosion of the coating over time. Salt spray tests were conducted in a 5% NaCl salt spray environment for 10 days, with regular observations of surface degradation of

the coated steel specimens and comparisons with blank controls to quantify the impact of different processing methods and coating formulations on long-term protective performance.

2 | Establishment of a system for different metal protective coating treatment methods and performance characterization methods

2.1 | Classification of titanium alloy surface treatment technologies

2.1.1 | Chemical treatment technology

Chemical treatment technology involves the reaction between the surface of titanium alloys and chemical reagents to form protective oxide films or other functional coatings on the material surface. In recent years, high-concentration NaOH or H_2O_2 treatment processes have been widely applied in the field of titanium alloy surface treatment, as these processes can form stable surface oxide layers. In the biomedical field, a method combining acid-base pretreatment with immersion in a rapid calcification solution (FCS) can form a bio-ceramic coating on the surface of TC4 titanium alloys. To further enhance coating performance, researchers introduced modifiers such as vinyl triethoxysilane and sodium polyacrylate to optimize the structural properties of the bio-ceramic coating. Chemical treatment offers advantages such as simplicity and low cost compared to other surface treatment methods. However, the oxide layers obtained through traditional chemical oxidation are relatively thin, and the dense oxide layers formed on the surface of titanium alloys can affect the effectiveness of subsequent chemical plating and electroplating processes. This liquid-phase deposition technology provides a new technical approach for the application of titanium alloys in the field of hard tissue implant materials.

2.1.2 | Heat treatment technology

Heat treatment technology alters the physical and chemical properties of titanium alloy surfaces by applying different temperature conditions and controlling cooling methods. Among these, laser hardening, as a localized heat treatment method, can refine the surface microstructure and enhance the hardness of titanium alloys. In practical applications, laser cladding technology demonstrates unique advantages, particularly in the treatment of friction pairs made of titanium alloys and nickel-based alloys in aircraft engines. By cladding the surface of the titanium alloy substrate with mechanically mixed powders of CoCrW and WC, a stable surface modification layer can be obtained in a short time. This technology features a short preparation cycle and stable quality, and effectively avoids cracking issues caused by thermal effects. Additionally, heat treatment of copper alloy coatings at temperatures below 600°C is another effective method, providing more technical options for regulating material surface properties.

2.1.3 | Electrochemical treatment technology

Electrochemical treatment technology is an important method for surface modification of titanium alloys, primarily including traditional anodizing and micro-arc oxidation (MAO) processes. MAO technology is a novel surface treatment method developed based on traditional anodizing, which overcomes the limitations of conventional anodizing by applying high voltage. This technology utilizes the instantaneous high-temperature

and high-pressure environment in the micro-arc discharge zone to directly convert the surface of titanium alloys into an oxide ceramic film. In micro-arc oxidation treatment of TC4 titanium alloy surfaces, a hard oxide film with excellent adhesion can be formed, achieving a surface hardness of approximately 417 HV, a significant improvement over the 204 HV hardness of untreated TC4 titanium alloy surfaces. Its corrosion resistance is also enhanced by approximately 51.08%. This electrochemical treatment method not only improves the wear resistance and corrosion resistance of the titanium alloy but also enhances the material's thermal shock resistance.

2.2 | Sample characterization

After modifying the surface of the metal substrate using the above chemical, heat treatment, and electrochemical techniques, it is necessary to systematically characterize the treated samples and the resulting coating/substrate interface in order to gain a deeper understanding of the treatment effects and their potential impact on the performance of subsequent coatings.

2.2.1 | Phase composition and microstructure

1) *Phase and composition analysis.* An RAX-10 X-ray diffractometer was used to characterize the phase composition of the surface of the molten salt-treated samples. The sample surface was scanned using Cu target Kα rays (λ = 1.5518 Å) over a range of 10 to 90°, at a speed of 10°/min.
2) *Morphology analysis.* An optical microscope (CX40M model) was used to test and characterize the macroscopic morphology of the samples after surface treatment. An S-4800 scanning electron microscope was used to test the surface before and after treatment, as well as the interface between the substrate and coating, and to characterize the surface, cross-section, and section morphology. An energy dispersive spectrometer attached to an EMPA-870QH2 electron probe was used to analyze the elemental distribution at the substrate-coating interface in face-scanning mode, thereby determining the chemical composition at the interface.

2.2.2 | Performance testing

1) *Substrate Surface Roughness.* Substrate surface roughness is one of the key factors influencing the surface condition of the substrate material and is also a primary factor affecting the adhesion between the coating and the substrate. The TIME@3221 surface roughness meter was used to characterize the average values of the Ra and Rmax roughness parameters of the substrate surface. Assemble the instrument, place the test sample on the stage, and control the movement of the sensor to slide it across the sample surface. After the sliding is complete, the sliding trajectory and roughness values are displayed on the roughness tester interface, and the Ra and Rmax values at this time are recorded as the results of a single test. The measurement length is 5.00 mm. Select 5-6 different points on the sample surface for measurement, then take the average value as the Ra value and Rmax value of the substrate's surface roughness.
2) *Substrate Vickers hardness.* A HDX-1000 TMC/LCD digital microhardness tester is used to characterize the Vickers hardness value of the substrate material. The computer performs indentation testing on the polished cross-section of the specimen. The procedure involves placing the specimen on the hardness tester's specimen stage, rotating the handwheel until a clear image appears on the computer screen, then performing

an indentation and recording the hardness value at that time. The loading force used in the test is 4.80 N, with a loading time of 10 seconds. Ten different positions are selected on the specimen surface for measurement, and the average value of the measurements is taken as the Vickers hardness value of the matrix.

2.2.3 | Interface integration performance

1) *Scratch test.* The MFT-4000 multifunctional material surface performance tester was used to conduct scratch tests on the interface between the substrate and the coating. The specific steps were as follows: the test sample was placed directly below the specimen stage, and the distance between the specimen on the stage and the scratch tester was adjusted using a computer to bring them close together. The scratch test was then initiated via the computer. The relevant parameters for the scratch test are as follows: the loading speed is set to 100 N/mm, the scratch length is set to 5 mm, and the scratch termination load is set to 100 N. Five scratch test results are taken for each sample to ensure the accuracy of the experimental results.
2) *Indentation test.* A digital microhardness tester is used to perform indentation tests on the interface between the substrate and the coating. The loading force used in the test is 4.80 N, and the loading time is 10 seconds. A computer was used to perform indentation tests on the interface between the coating and substrate of the specimens. The procedure involved placing the specimen on the hardness tester's specimen stage, rotating the handwheel until a clear image appeared on the computer screen, and then performing one indentation test on the specimen. Five indentation results were obtained for each specimen.
3) *Tensile test.* A 5583-type universal testing machine was used to determine the bond strength between the substrate and the coating interface. The specific operation process was as follows: one side of the specimen was coated, and the other side was surface-treated, with the specimen dimensions being ϕ=26.1 mm. E7 adhesive was then applied to both sides of the specimen, and two molds were selected to bond with both sides of the specimen, forming one pair of specimens. Ensure good alignment between the two, then apply pressure to fix them in place. Use a scalpel to remove any excess adhesive from the specimen's surface, then place the specimen in an oven and dry it at 100°C for 3 hours. The specimen is then removed and placed in a testing machine. The testing machine is operated via computer until the specimen separates from the mold, at which point the value is recorded. To ensure the accuracy of the test results, five pairs of specimens are selected from each group, and their bond strength values are tested. The average value is taken as the bond strength.

2.3 | Performance testing

Based on the results of the microstructural characterization and interfacial adhesion performance tests described above, this chapter further conducts standardized tests on the key properties of the coating itself—adhesion, toughness, and corrosion resistance—to evaluate the practical application performance of the metal protective coatings prepared using different surface treatment methods.

2.3.1 | Adhesion test

Conduct adhesion testing on the prepared coating. First, apply an equal amount of AB adhesive evenly to the test specimen in the testing instrument and let it cure for 24 hours. The test specimen with the coating is securely attached to the adhesion tester. A vertical tensile stress is applied to the test specimen, with the stress increasing at a constant rate of 0.6 MPa/s. When the adhesion between the test specimen and the coating

reaches its maximum value, the adhesion tester records the measured data. The measurement is repeated 10 times, and the average value is taken to minimize errors.

2.3.2 | Resilience testing

Conduct a toughness test on the prepared coating. After assembling the coating toughness tester, select the appropriate shaft size for the coating being tested (typically tested in descending order from largest to smallest). Secure the coating to be tested to the bottom of the shaft, rotate the handle 180 degrees to ensure the shaft comes into contact with the coating, and finally inspect whether the bent coating has cracked. When the coating surface cracks, the previous shaft size is considered the coating's optimal toughness. After determining the optimal toughness, five tests must be conducted to minimize errors.

2.3.3 | Chloride salt immersion test

Corrosion resistance testing of polymeric anti-corrosion coatings. Three samples were prepared for each formulation and cured in a constant temperature and humidity chamber for 144 hours. After curing, the edges and backs of the specimens were sealed. The polymer corrosion-resistant coating specimens to be tested were immersed in a 3.0% sodium chloride solution, and the corrosion condition of the coating surface was observed after 1 day, 5 days, and 10 days, respectively. The results were compared with the control group to determine the effect of different treatment methods on the corrosion resistance of the polymer coating.

2.3.4 | Salt spray test

Conducting salt spray corrosion resistance testing. Use oxalic acid to clean rust from the surface of steel bars with a diameter of 7.5 mm and a length of 15 cm, then use ethanol to remove any excess oxalic acid from the steel bars. The prepared polymer corrosion-resistant coating was then evenly applied to the surface of the steel bars using a brush. Three samples were prepared for each formulation, which were cured under constant temperature and humidity conditions for 168 hours. The ends of the steel bars were then sealed with epoxy resin, and after drying for 1 day, the samples were placed in a salt spray chamber with a sodium chloride concentration of 5%. Conduct a salt spray test for 10 consecutive days. On the 10th day, observe the changes on the surface of the titanium alloy coated with the polymer corrosion-resistant coating to assess the impact of different treatment methods on the corrosion resistance of the titanium alloy coating.

3 | Research on the stability and protective performance of coating structures in titanium alloy surface treatment processes

Based on the surface treatment technology system and characterization methods established in previous section focuses on TC4 titanium alloy to systematically conduct multi-scale performance verification of coating corrosion protection under chemical treatment, heat treatment, and electrochemical treatment, and to investigate the influence mechanism of different treatment processes on the structure-function characteristics of the coating.

3.1 | Chemical pretreatment of TC4 titanium alloy substrate and preparation of SiO_2 coating

3.1.1 | Pre-treatment of substrate surface

Using titanium alloy TC4 as the experimental subject, the TC4 substrate was ultrasonically cleaned with deionized water and anhydrous ethanol for 30 minutes, followed by three rinses with deionized water for later use.

Five solutions were used for immersion at 150°C for 1 hour: high-concentration NaOH, H_2O_2, fast calcification solution (FCS), vinyl triethoxysilane (C_8HO_3Si), and sodium polyacrylate $(C_3H_3NaO_2)_n$. After cooling to room temperature, the samples were removed and rinsed with deionized water.

3.1.2 | Coating preparation

Take 50 mL of anhydrous ethanol and place it in a beaker. Add 4.531 g of ethyl orthosilicate, stir for 5 minutes to ensure uniform mixing, and label as A. Take another 50 mL of anhydrous ethanol, add 2 mL of deionized water and 0.04 mL of hydrochloric acid, mix thoroughly, and label as B. Using a separatory funnel, slowly add solution B to solution A, stir at 26°C room temperature for 1 hour, at a speed of 300 rpm, and then aged at 70°C in an oven for 6 hours to obtain the SiO_2 sol-gel coating solution. The surface-treated TC4 substrate was vertically and slowly immersed into the SiO_2 sol-gel coating solution, and the coating was slowly and uniformly lifted at a speed of 4 cm/min, repeated five times, and then dried and set aside for later use.

3.1.3 | Experimental procedure

Irradiation test: UV irradiation (280-350 nm) at a temperature of 40°C, irradiation intensity of 1 W/m^2, for 72 hours.

During heat treatment, the cleaned TC4 substrate was subjected to experimental treatment using either 100°C hydrothermal treatment or 600°C vacuum heating.

3.2 | Effect of surface treatment on the optical properties of coatings and the structural stability of substrates

After completing the substrate pretreatment and coating preparation, it is necessary to systematically evaluate the impact of different treatment processes on the functional properties of the coating (such as optical performance) and the structural stability of the substrate.

3.2.1 | Analysis of optical properties after chemical treatment

Figure 1 shows the changes in transmittance of TC4 coated with a SiO_2 layer before and after 72 hours of UV irradiation, following surface modification using different methods. As shown in the figure, except for the TC4 substrate pretreated with H_2O_2 solution, which exhibited a slight decrease in transmittance, the transmittance of TC4 coated with SiO_2 after surface modification using the other four methods remained unchanged after 72 hours of irradiation. This indicates that the coating samples prepared using NaOH, H_2O_2, FCS, C_8HO_3Si, and $(C_3H_3NaO_2)_n$ chemical treatments maintained good optical properties and demonstrated a certain degree

of resistance to UV irradiation after 72 hours of UV exposure.

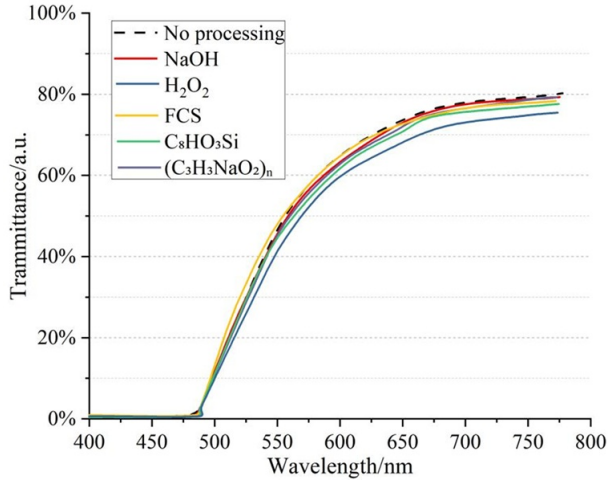

FIGURE 1 Transmittance curves of silica coated TC4 before and after UV irradiation

3.2.2 | FTIR analysis after heat treatment

Figure 2 shows the FTIR spectra of TC4 before and after hydrothermal treatment and vacuum treatment. From the curves in the figure, it can be observed that after 1 hour of hydrothermal treatment at 100°C, the characteristic absorption peaks of the imine ring, including the carbonyl stretching vibration peak at 1017 nm, the C-N stretching vibration peak at 1434 nm, and the aromatic ring stretching vibration peaks at 1910 nm, 1933 nm. This indicates that the overall structure of TC4 remains unchanged under these hydrothermal conditions and after vacuum treatment at 600°C.

During vacuum heating treatment at 600°C, the thickness of the oxide layer on the surface of the TC4 substrate was only one-fifth of that obtained under air treatment. This dense oxide film significantly enhances the material's corrosion resistance in marine environments. High-frequency induction heat treatment technology, through rapid heating and controlled cooling, can form a nanocrystalline layer on the surface of titanium alloys.

3.3 | XRD phase analysis

The above optical performance and structural stability analysis indicate that different processing methods have a significant impact on the surface of TC4 and the interface state between the coating and substrate. To further clarify its phase composition and phase transformation behavior, especially the differences in phase composition after high-temperature cycling, in-depth phase analysis using X-ray diffraction (XRD) is required.

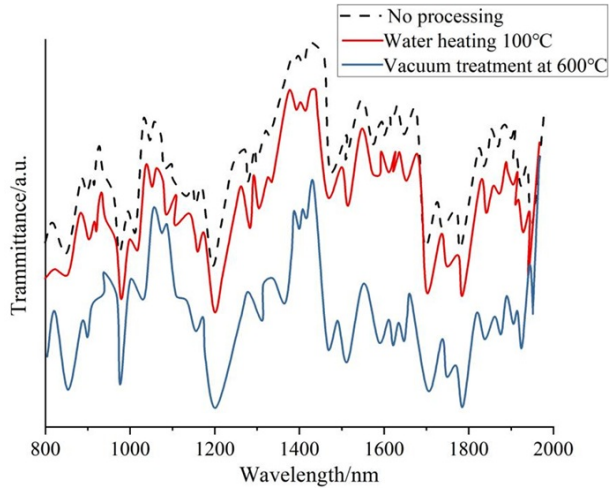

FIGURE 2 FTIR spectra of TC4 of hydrothermal and Vacuum heating treatment

3.3.1 | XRD phase analysis under different chemical treatments

The TC4 titanium alloy treated with five solutions—NaOH, H_2O_2, fast calcium solution (FCS), vinyl triethoxysilane (C_8H_3Si), and sodium polyacrylate $(C_3H_3NaO_2)_n$—was subjected to 200 cycles at room temperature, heat treatment at 100°C, and vacuum heat treatment at 600°C. The XRD diffraction patterns obtained are shown in Figures 3–7. It can be seen that the phase composition of the high-temperature alloy before oxidation is γ/γ' phase for all five solutions, while the phase composition after oxidation shows significant differences.

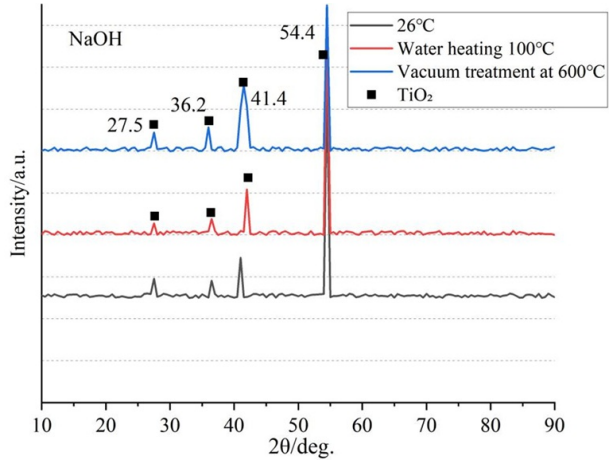

FIGURE 3 XRD patterns of X after being treated with NaOH solution

It can be seen that under NaOH treatment, the main oxidation product is rutile-type TiO_2, with strong peaks at 27.5° (110) and 36.2° (101). Characteristic peaks also appear at 41.4° and 54.5°, indicating that high-temperature cycling promotes the phase transformation from anatase to rutile.

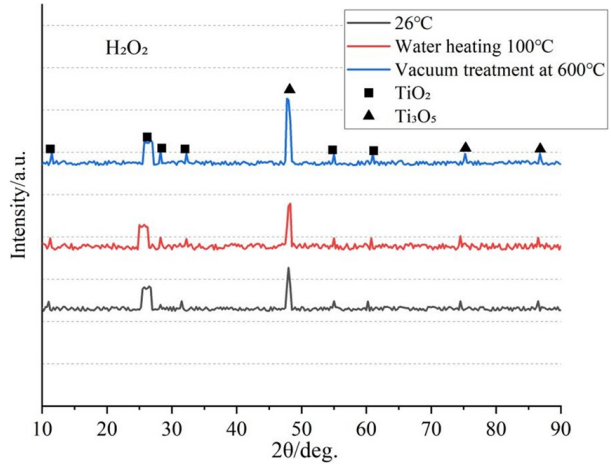

FIGURE 4 XRD patterns of X after being treated with H_2O_2 solution

Under H_2O_2 treatment, the oxidation products are amorphous TiO_2 + Ti_3O_5. The 25.6° broad peak is characteristic of amorphous TiO_2, while the 48.2° peak corresponds to Ti_3O_5. The loose H_2O_2 oxide film leads to the formation of some sub-stoichiometric oxides.

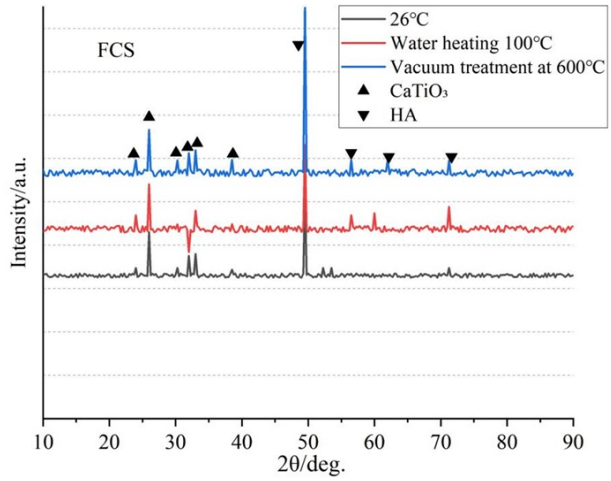

FIGURE 5 XRD patterns of X after being treated with FCS solution

The oxidation products under FCS treatment are $CaTiO_3$ and hydroxyapatite $Ca_{10}(PO_4)_6(OH)_2$. The 33.2° peak corresponds to the $CaTiO_3$ (121) crystal plane, while the 25.9° and 31.8° peaks correspond to the (002) and (211) crystal planes of HA, respectively. FCS pre-calcination promotes the formation of the perovskite structure.

The oxidation products of vinyl triethoxysilane are amorphous SiO_2 + Ti_5Si_3. The 22° broad peak corresponds to the amorphous characteristic of SiO_2, while the 35.5° peak corresponds to the Ti_5Si_3(112)

crystal plane. At high temperatures, Si reacts with Ti to form silicides.

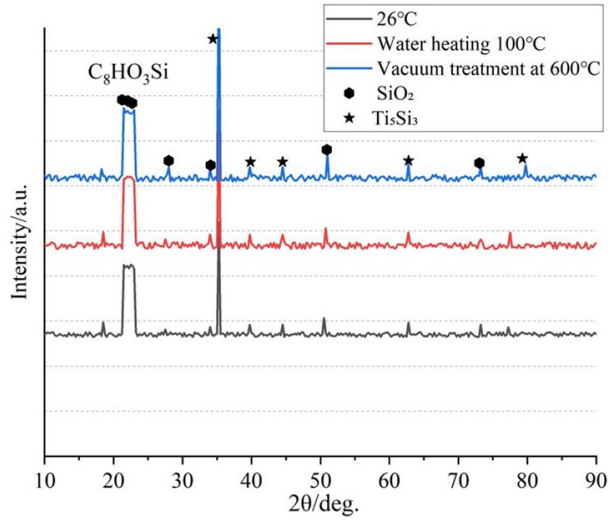

FIGURE 6 XRD patterns of X after being treated with C_8HO_3Si solution

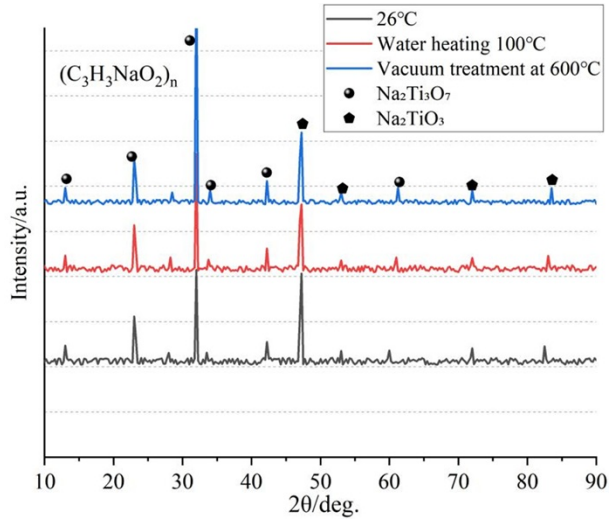

FIGURE 7 XRD patterns of X after being treated with $(C_3H_3NaO_2)_n$ solution

The products obtained under sodium polyacrylate treatment are $Na_2Ti_3O_7$ and Na_2TiO_3. The characteristic peaks of $Na_2Ti_3O_7$ are at 23.8° (110) and 32.7° (020), while the peak at 47.1° is attributed to Na_2TiO_3. Na^+ ions are embedded into the titanium oxide structure to form layered compounds.

The antioxidant activity ranking is FCS > silane > NaOH > sodium polyacrylate > H_2O_2. The FCS group forms a dense $CaTiO_3$/HA composite layer, resulting in the slowest decrease in γ-Ti peak intensity

(lowest oxidation level); the H_2O_2 group shows nearly complete disappearance of the γ-Ti peak, with the weakest protective properties of the amorphous oxide layer. High-temperature phase stability is reflected in the enhanced Ti_5Si_3 peak at 600°C in the silane-treated group, with silicates inhibiting oxygen diffusion.

3.3.2 | XRD phase analysis under electrochemical treatment

The aforementioned analysis focuses on the effects of chemical treatment and heat treatment on phase composition. Correspondingly, as an important surface modification technique, the phase composition of the coatings induced by electrochemical treatment also requires detailed analysis.

The XRD diffraction patterns of the alloy treated with traditional anodization and micro-arc oxidation (MAO) are shown in Figure 8. Before oxidation, both coatings consist of a saturated single γ phase, with other elements present in the γ phase in the form of solid solutions.

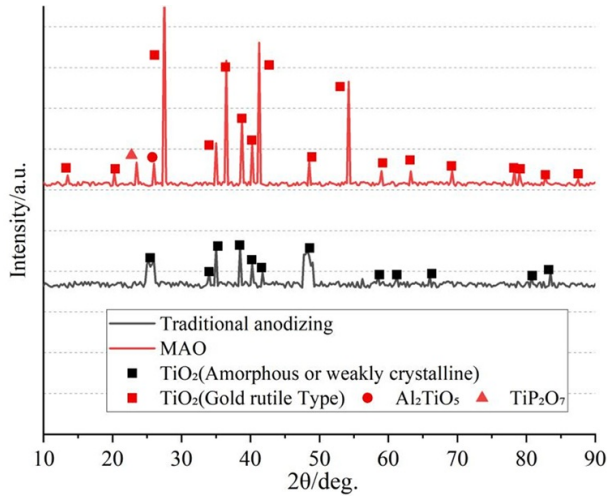

FIGURE 8 XRD patterns after traditional anodizing and MAO treatment

Under conventional anodization, the main product is amorphous or weakly crystalline TiO_2 (primarily the anatase phase), characterized by broadened peak widths and low intensity, with typical peaks at 25.3° and 48.1°. The α-Ti phase of the substrate (with main peaks at 35.1°, 38.4°, and 40.2°) remains significantly present, indicating a thin oxide film.

Under micro-arc oxidation (MAO), the oxidation products are highly crystalline rutile-type TiO_2, with sharp and high-intensity characteristic peaks, with strong peaks at 27.5° (110), 36.1° (101), 41.2° (111), and 54.3° (211). Due to the composition of the electrolyte (e.g., containing silicates or phosphates), small amounts of Al_2TiO_5 (peak at 26.1°) or TiP_2O_7 (peak at 23.5°) may be formed, enhancing the stability of the coating layer. The intensity of the α-Ti peak is significantly reduced, indicating a thicker and denser oxide film.

Chemical composition analysis of the TC4 titanium alloy coatings under the two electrochemical treatment technologies was conducted, with seven points randomly selected as observation points. Table 1 shows the chemical composition analysis of the coatings at each point under the two treatment methods.

Table 1 presents the chemical composition (Ti, O, C, Al, Si, P) and their average values at seven randomly

selected points (P1–P7) on the surface of TC4 titanium alloy coatings treated with traditional anodizing and micro-arc oxidation (MAO). The data clearly reveal significant differences in elemental composition between the coatings formed by the two treatment technologies.

TABLE 1 Chemical composition analysis of each point of the coating/%

	Traditional anodizing				MAO			
	Ti	O	C	Al	Ti	O	Si	P
P1	58.24	8.52	1.23	0.88	50.44	13.64	2.06	2.15
P2	58.33	7.89	1.05	0.94	48.96	15.17	1.98	2.02
P3	57.92	6.73	1.32	0.70	51.21	12.85	2.31	1.42
P4	59.16	9.21	1.15	0.99	51.97	16.33	1.75	2.34
P5	59.59	8.14	0.97	0.96	49.47	14.08	2.54	2.12
P6	58.22	7.62	1.41	0.72	51.95	13.17	2.22	1.72
P7	58.01	9.05	1.08	1.09	48.26	16.95	1.63	2.45
Average	58.50	8.17	1.17	0.90	50.32	14.60	2.07	2.03

In the traditional anodizing coating, the primary component is titanium (Ti), with an average content as high as 58.50%, while the average oxygen (O) content is relatively low at 8.17%. Additionally, it contains small amounts of carbon (C), averaging 1.17%, and aluminum (Al), averaging 0.90%. The content fluctuations of each element at different measurement points are relatively small, indicating that the coating composition is relatively uniform but dominated by the titanium substrate. The extremely high titanium content and extremely low oxygen content indicate that the formed titanium dioxide (TiO_2) film layer is very thin and unable to effectively cover the substrate.

In the micro-arc oxidation (MAO) coating, the titanium (Ti) content is significantly reduced, averaging 50.32%, while the oxygen (O) content is significantly increased, averaging 14.60%, indicating the formation of a thicker, more oxidized surface layer. Additionally, the coating contains significant amounts of silicon (Si) at 2.07% and phosphorus (P) at 2.03%, elements that are virtually absent in traditional anodized coatings. These Si and P elements originate from the electrolyte (e.g., silicates, phosphates) and are incorporated into the growing ceramic layer under the high-temperature, high-pressure conditions of micro-arc discharge, forming phases such as Al_2TiO_5 and TiP_2O_7. There is some variation in elemental content across different measurement points, which may reflect the non-homogeneous microstructure of the ceramic layer, such as micro-pores and melted particles. This composition, rich in oxygen and titanium and containing electrolyte-derived elements (Si, P), is direct evidence of the formation of a thick, composite ceramic oxide film in MAO.

3.4 | Analysis of metal coating performance test results under different treatment methods

XRD phase analysis revealed the phase composition evolution at the coating/substrate interface under different treatment processes. Based on this, Section 3.4 further combines mechanical and electrochemical tests to quantify the contribution of the above phase characteristics to coating adhesion and corrosion resistance.

3.4.1 | Coating adhesion test analysis

Different methods were used to treat the surface of TC4 titanium alloy. After treatment, the surface roughness of the test samples was measured. At the same time, epoxy anti-rust paint was applied to the surface of the samples. The adhesion of the coating on the samples after different surface treatments was tested. The average results of 10 tests are shown in Table 2.

TABLE 2 Test results of adhesion of coatings after different surface treatments

		Surface roughness/μm	Adhesion strength/MPa	Interface failure mode
Chemical treatment	NaOH	29	3.47	70%A/B
	H_2O_2	16	2.57	90%A/B
	FCS	60	7.83	100%B
	C_8HO_3Si	63	8.01	100%B
	$(C_3H_3NaO_2)_n$	42	5.15	40%A/B
	Hydrothermal treatment 100℃	34	4.85	60%A/B
	Vacuum heating 600℃	52	6.72	20%A/B
Electrochemical treatment	Traditional anodizing	38	4.16	60%A/B
	MAO	62	7.91	100%B

As shown in Table 2, the surface treatment grade of the substrate is correlated with surface roughness. The higher the roughness, the larger the contact area between the coating and the substrate, resulting in higher coating adhesion strength. Among chemical treatments, the substrate treated with vinyl triethoxysilane exhibited the highest roughness (63 μm), corresponding to the strongest coating adhesion (8.01 MPa); while H_2O_2 treatment resulted in the lowest roughness of 16 μm and the weakest adhesion (2.57 MPa). Therefore, the surface of TC4 titanium alloy substrates should be pretreated with a C_8HO_3Si solution immersion to remove surface contaminants while achieving a surface roughness of over 60 μm, thereby ensuring the substrate surface protective coating has excellent adhesion strength.

The coatings treated with FCS, C_8HO_3Si, and micro-arc oxidation (MAO) all exhibited 100% Type B failure, indicating cohesive failure within the coating, which suggests that the interfacial bond strength is higher than the coating's own strength. In contrast, H_2O_2 and hydrothermal treatment at 100°C primarily resulted in A/B-type failure (mixed failure), indicating weaker interfacial bonding. MAO treatment exhibited an adhesion strength of 7.91 MPa, which is comparable to that of C_8HO_3Si treatment (8.01 MPa) and significantly superior to the 4.16 MPa of traditional anodic oxidation.

3.4.2 | Analysis of the surface potential of the substrate

Studies have shown that immersion in FCS and C_8HO_3Si solutions can effectively increase the surface roughness of the substrate, ensuring the adhesion strength of the coating on the substrate surface. However, due to the unique chemical composition of the TC4 titanium alloy surface, the residuals of different solutions on the substrate surface can significantly affect the corrosion resistance of the substrate surface. FCS, $_8HO_3Si$, and $(C_3H_3NaO_2)_n$ solutions, which demonstrated overall superior performance, were used to treat the titanium alloy surface. The surface potential of the treated TC4 titanium alloy was tested. The results of the surface polarization potential tests and the electrochemical characteristics of the substrate surface under the three

solution immersion treatments are shown in Figure 9 and Table 3, respectively.

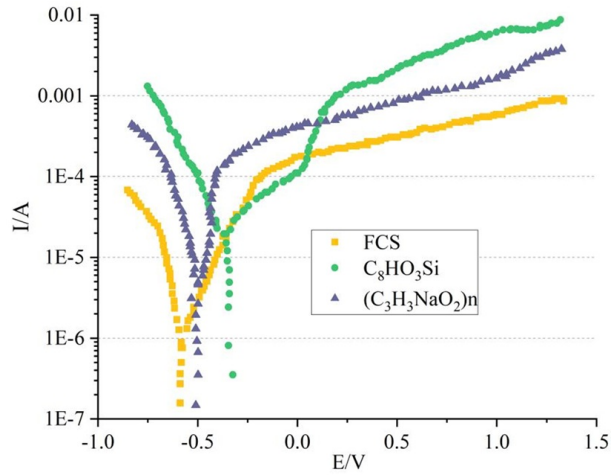

FIGURE 9 Surface polarization potential maps of TC4 under 3 different treatments

TABLE 3 Electrochemical characteristic values of the surface of TC4 titanium alloy

	FCS	C_8HO_3Si	$(C_3H_3NaO_2)_n$
Open Circuit Potential (OCP)/V	-0.281	-0.173	-0.234
Corrosion Potential/V	-0.168	-0.087	-0.121
Corrosion Current (nA/cm^2)	30.7	4.3	13.9
Passivation Potential/V	0.837	0.876	0.851
Breakdown Potential/V	0.945	0.962	0.952
Passivation Zone Width/V	0.118	0.131	0.124
Passivation Current Density (μA/cm^2)	1.316	0.451	0.768

The more positive the self-corrosion potential of a metal, the wider the passivation zone, and the more corrosion-resistant the metal. As shown in Figure 9 and Table 3, compared to treatments with FCS and $(C_3H_3NaO_2)_n$, titanium alloys treated with C_8HO_3Si solution exhibit superior corrosion resistance. The corrosion potential of C_8HO_3Si treatment is the most positive (-0.087 V), the corrosion current is the lowest (4.3 nA/cm^2), the passivation potential range is the widest (0.131 V), and the passivation current density is the smallest (0.451 μA/cm^2). Under FCS treatment, the corrosion current (30.7 nA/cm^2) is significantly higher than that of C_8HO_3Si, indicating poorer corrosion resistance. Sodium polyacrylate exhibits an intermediate performance, with corrosion potential (-0.121 V) and current (13.9 nA/cm^2) between the two, but a narrower passivation range (0.124 V).

3.4.3 | Electrochemical impedance test results and analysis

The electrochemical impedance of the coating system determines the penetration and diffusion performance of the corrosive medium within the coating. The higher the electrochemical impedance, the better the coating's shielding performance against the corrosive medium, i.e., the higher the coating's corrosion resistance. The electrochemical impedance test results of the coating systems on titanium alloy surfaces under different treatment conditions are shown in Figure 10.

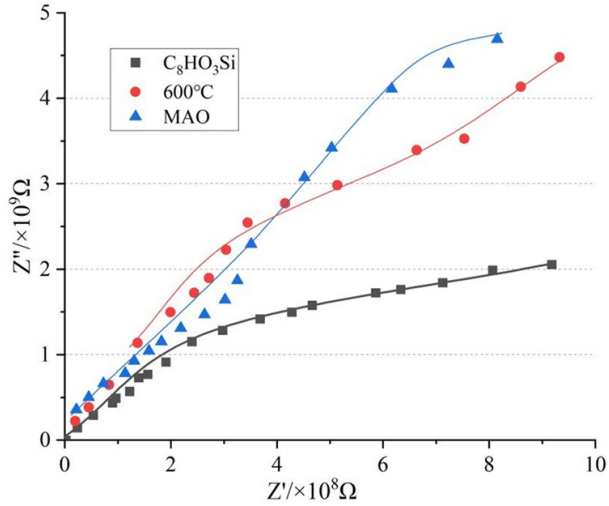

FIGURE 10 The conditions of different coating systems after 10d of salt spray testing

As shown in Figure 10, after 10 days of conventional salt spray testing, the electrochemical impedance of all coating systems remained above 1.0×10^9, indicating that the coatings formed on the surface of TC4 titanium alloy after chemical treatment with C_8HO_3Si solution, vacuum heating at 600°C, and MAO micro-arc oxidation electrochemical treatment all exhibit excellent shielding effects against corrosive media, demonstrating superior corrosion resistance.

4 | Conclusion

This study systematically compared the effects of three types of surface treatment methods (chemical, thermal, and electrochemical) on the performance of protective coatings for TC4 titanium alloy, leading to the following conclusions.

Dense oxide layers (e.g., rutile TiO_2 in MAO and $CaTiO_3$/hydroxyapatite in FCS) can significantly inhibit the penetration of corrosive media. High-temperature thermal treatment (600°C under vacuum) forms a thin oxide layer (one-fifth the thickness in air), which synergistically enhances the structural stability of the substrate. FTIR analysis confirmed that the characteristic peaks remained unchanged.

Surface roughness is the core factor determining coating adhesion. Chemical treatment with vinyl triethoxysilane (C_8HO_3Si) achieved the highest surface roughness (63 μm), corresponding to a coating adhesion strength of 8.01 MPa, with a failure mode of 100% Type B (coating cohesive failure), indicating that the

interfacial bonding strength exceeds the coating's own strength. Micro-arc oxidation (MAO) treatment achieved a roughness of 62 μm and adhesion of 7.91 MPa, comparable to C_8HO_3Si, and significantly superior to the 4.16 MPa achieved by traditional anodic oxidation.

The C_8HO_3Si-treated samples exhibited the most positive corrosion potential (-0.087 V), the lowest corrosion current (4.3 nA/cm^2), the widest passivation range (0.131 V), the smallest passivation current density (0.451 μA/cm^2), and the best corrosion resistance. MAO treatment formed a highly crystalline rutile-type TiO_2 ceramic layer (characteristic peaks at 27.5° and 36.1°), increasing surface hardness to 417 HV and improving corrosion resistance by 51.08%; After 10 days of salt spray testing, the impedance remained $>1.0\times10^9\ \Omega\cdot\text{cm}^2$. Although FCS treatment exhibits strong adhesion (7.83 MPa), residual calcium salts cause elevated corrosion current (30.7 nA/cm^2), limiting corrosion resistance.

References

[1] Kania, H. (2023). Corrosion and anticorrosion of alloys/metals: the important global issue. *Coatings, 13*(2), 216.

[2] Fu, Y., Li, J., Luo, H., Du, C., & Li, X. (2021). Recent advances on environmental corrosion behavior and mechanism of high-entropy alloys. *Journal of Materials Science & Technology, 80*, 217-233.

[3] Prasad, A. R., Kunyankandy, A., & Joseph, A. (2020). Corrosion inhibition in oil and gas industry: Economic considerations. *Corrosion Inhibitors in the Oil and Gas Industry*, 135-150.

[4] Koch, G. (2017). Cost of corrosion. *Trends in Oil and Gas Corrosion Research and Technologies*, 3-30.

[5] Bender, R., Féron, D., Mills, D., Ritter, S., Bäßler, R., Bettge, D., ... & Zheludkevich, M. (2022). Corrosion challenges towards a sustainable society. *Materials and Corrosion, 73*(11), 1730-1751.

[6] Melchers, R. E. (2018). A review of trends for corrosion loss and pit depth in longer-term exposures. *Corrosion and Materials Degradation, 1*(1), 42-58.

[7] Lenhoff, T. (2024). Energy-preserving optimal control of multibody systems via advanced direct transcription methods. *TK Techforum Journal (ThyssenKrupp Techforum), 2024*(2), 15–24.

[8] Guo, S., Leavitt, J. J., Zhou, X., Xie, Y., Tietze, S., Zhu, Y., ... & Zhang, J. (2017). Effects of flow, Si inhibition, and concurrent corrosion of dissimilar metals on the corrosion of aluminium in the environment following a loss-of-coolant accident. *Corrosion Science, 128*, 100-109.

[9] Canturri, C., Salim, Y. S., Pivdiablyk, I., & Sing, S. L. (2024). Failure analysis of thermoplastic composites subject to galvanic corrosion in hybrid metal–composite joints. *Engineering Failure Analysis, 164*, 108405.

[10] Daood, S. S., Ottolini, M., Taylor, S., Ogunyinka, O., Hossain, M. M., Lu, G., ... & Nimmo, W. (2017). Pollutant and corrosion control technology and efficient coal combustion. *Energy & Fuels, 31*(5), 5581-5596.

[11] Ali, M., Ul-Hamid, A., Khan, T., Bake, A., Butt, H., Bamidele, O. E., & Saeed, A. (2021). Corrosion-related failures in heat exchangers. *Corrosion Reviews, 39*(6), 519-546.

[12] Yan, L., Xiao, K., Yi, P., Dong, C., Wu, J., Bai, Z., ... & Li, X. (2017). The corrosion behavior of PCB-ImAg in industry polluted marine atmosphere environment. *Materials & Design, 115*, 404-414.

[13] Alagi, P., Ghorpade, R., Choi, Y. J., Patil, U., Kim, I., Baik, J. H., & Hong, S. C. (2017). Carbon dioxide-based polyols as sustainable feedstock of thermoplastic polyurethane for corrosion-resistant metal coating. *ACS Sustainable Chemistry & Engineering, 5*(5), 3871-3881.

[14] Connor, E. J. (2024). Evaluation of bending properties in cold-formed stainless steel hollow sections. *TK Techforum Journal (ThyssenKrupp Techforum), 2024*(2), 25–31.

[15] Olajire, A. A. (2018). Recent advances on organic coating system technologies for corrosion protection of offshore metallic structures. *Journal of Molecular Liquids, 269*, 572-606.

[16] Wang, J., Hu, J., Gu, C., Mou, Y., Yu, J., & Zhong, X. (2022). The effect of pulse current cathodic protection on cathodic disbondment of epoxy coatings. *Progress in Organic Coatings, 170*, 107001.

[17] Petrunin, M. A., Maksaeva, L. B., Gladkikh, N. A., Yurasova, T. A., Maleeva, M. A., & Ignatenko, V. E. (2021). Cathodic delamination of polymer coatings from metals. Mechanism and prevention methods. A review. *International Journal of Corrosion and Scale Inhibition, 10*(1), 1-28.

[18] Yang, C., Han, Q., Wang, A., Yang, Y., & Li, X. (2021). Protection-failure mechanism of alkalinization and cathodic protection focusing on coating/metal interfaces. *AIP Advances, 11*(3), 035217.

[19] Wirtanen, T., Prenzel, T., Tessonnier, J. P., & Waldvogel, S. R. (2021). Cathodic corrosion of metal electrodes—how to prevent it in electroorganic synthesis. *Chemical Reviews, 121*(17), 10241-10270.

[20] Seo, J. S., Jeon, H. T., & Han, T. H. (2021). Peeling mechanism of interlocked interface between etched acrylonitrile-butadiene-styrene and electroplated metal layer. *Surfaces and Interfaces, 26*, 101337.

[21] Zhang, X., Zhang, Y., Zhou, Q., Zhang, X., & Guo, S. (2019). Symmetrical "sandwich" polybutadiene film with high-frequency low dielectric constants, ultralow dielectric loss, and high adhesive strength. *Industrial & Engineering Chemistry Research, 59*(3), 1142-1150.

[22] Yue, Y., Wang, W. W., Zhang, L., Liang, L., & Zhao, Q. (2024). Effect of sand coating on durability and micro-structural deterioration of GFRP rebar under alkaline environment attack. *Construction and Building Materials, 413*, 134900.

[23] Croll, S. G. (2020). Surface roughness profile and its effect on coating adhesion and corrosion protection: A review. *Progress in organic Coatings, 148*, 105847.

[24] Luo, Y., Li, X., Luo, Z., Chen, L., Yang, Y., Li, J., & Han, G. (2023). Enhanced adhesive and anti-corrosive performances of polymer composite coating for rusted metallic substrates by capillary filling. *Progress in Organic Coatings, 178*, 107467.

[25] Akbarzadeh, S., Ramezanzadeh, M., & Ramezanzadeh, B. (2020). Inspection the corrosion prevention performance and dry/wet interfacial adhesion qualities of the melamine-cured polyester coating applied on the treated mild steel surface with a nanostructured composite cerium-neodymium film. *Colloids and Surfaces A: Physicochemical and Engineering Aspects, 590*, 124472.

[26] Baek, I., Lim, C. M., Park, K. Y., & Ryu, B. K. (2022). Enhanced metal coating adhesion by surface modification of 3D printed PEKKs. *Coatings, 12*(6), 854.

[27] Caraguay, S. J., Pereira, T. S., Cunha, A., Pereira, M., & Xavier, F. A. (2023). The effect of laser surface textures on the adhesion strength and corrosion protection of organic coatings-Experimental assessment using the pull-off test and the shaft load blister test. *Progress in Organic Coatings, 180*, 107558.

[28] Fan, C., Wang, X., Yin, X., Huang, W., Da, Y., Jiang, H., ... & Zhang, W. (2023). Adhesion strength and anti-corrosion performance of ceramic coating on laser-textured aluminum alloy. *Coatings, 13*(12), 2098.

[29] Abdelaal, A. F., Samad, M. A., Adesina, A. Y., & Baig, M. M. A. (2022). Effect of plasma treatment on the tribological and adhesion performance of a polymer coating deposited on different metallic substrates. *Journal of Coatings Technology and Research, 19*(6), 1673-1686.

[30] Dong, H., Guo, P. F., Han, Y., Bai, R. X., Yang, Z. C., & Zhang, S. Q. (2023). Enhanced corrosion resistance of high speed laser-cladded Ni/316L alloy coating by heat treatment. *Journal of Materials Research and Technology, 24*, 952-962.

[31] Gao, S., Du, Y., Cong, M., He, Y., & Lei, W. (2024). The impact of ultrasonic shock surface treatment technology on the microstructure, mechanical and corrosion properties of FeCrMnCuNiSi high-entropy alloy coating via TIG arc melting. *Materials Today Communications, 41*, 110282.

[32] Wang, X. Z., Fan, H. Q., Muneshwar, T., Cadien, K., & Luo, J. L. (2021). Balancing the corrosion resistance and through-plane electrical conductivity of Cr coating via oxygen plasma treatment. *Journal of Materials Science & Technology, 61*, 75-84.

[33] Izadi, M., Shahrabi, T., & Ramezanzadeh, B. (2018). Active corrosion protection performance of an epoxy coating applied on the mild steel modified with an eco-friendly sol-gel film impregnated with green corrosion inhibitor loaded nanocontainers. *Applied Surface Science, 440*, 491-505.

[34] Parhizkar, N., Shahrabi, T., & Ramezanzadeh, B. (2017). A new approach for enhancement of the corrosion protection properties and interfacial adhesion bonds between the epoxy coating and steel substrate through surface treatment by covalently modified amino functionalized graphene oxide film. *Corrosion Science, 123*, 55-75.

[35] Ramezanzadeh, M., Sanaei, Z., & Ramezanzadeh, B. (2018). The influence of steel surface treatment by a novel eco-friendly praseodymium oxide nanofilm on the adhesion and corrosion protection properties of a fusion-bonded epoxy powder coating. *Journal of Industrial and Engineering Chemistry, 62*, 427-435.

[36] Mahidashti, Z., Shahrabi, T., & Ramezanzadeh, B. (2018). The role of post-treatment of an ecofriendly cerium nanostructure Conversion coating by green corrosion inhibitor on the adhesion and corrosion protection properties of the epoxy coating. *Progress in Organic Coatings, 114*, 19-32.

[37] Iqbal, M. A., Asghar, H., Matykina, E., Arrabal, R., Mohedano, M., & Vega, J. M. (2025). Synergy of consecutive PEO and LDH surface treatments on the corrosion protection and adhesion strength of organic coatings on AA2024T3. *Progress in Organic Coatings, 207*, 109397.

[38] Bahlakeh, G., Ramezanzadeh, B., & Ramezanzadeh, M. (2019). The role of chrome and zinc free-based neodymium oxide nanofilm on adhesion and corrosion protection properties of polyester/melamine coating on mild steel: experimental and molecular dynamics simulation study. *Journal of Cleaner Production, 210*, 872-886.

[39] Jothi, V., Adesina, A. Y., Rahman, M. M., Kumar, A. M., & Ram, J. N. (2020). Improved adhesion and corrosion resistant performance of polyurethane coatings on anodized Mg alloy for aerospace applications. *Journal of Materials Engineering and Performance, 29*(4), 2586-2596.

[40] Wang, R., Xu, H., Yao, Z., Li, C., & Jiang, Z. (2020). Adhesion and corrosion resistance of micro-arc oxidation/polyurethane composite coating on aluminum alloy surface. *Applied Sciences, 10*(19), 6779.

[41] Trentin, A., Samiee, R., Pakseresht, A. H., Durán, A., Castro, Y., & Galusek, D. (2023). Influence of pre-treatments on adhesion, barrier and mechanical properties of epoxy coatings: A comparison between steel, AA7075 and AA2024. *Applied Surface Science Advances, 18*, 100479.